Research Square

Preprints are preliminary reports that have not undergone peer review.
They should not be considered conclusive, used to inform clinical practice,
or referenced by the media as validated information.

A Targeted Spatial Transcriptomics Framework for a High-Resolution Human Skin Cell Atlas

Michael Peake

michael.peake@manchester.ac.uk

The University of Manchester https://orcid.org/0009-0007-5525-0401

Abigail Langton

The University of Manchester https://orcid.org/0000-0001-9567-9586

Mark Farrar

The University of Manchester https://orcid.org/0000-0001-8602-7279

Bezaleel Mambwe

The University of Manchester https://orcid.org/0000-0001-8751-1425

Orsolya Kiss

The University of Manchester

Wen Duan

The University of Manchester

Anne Chandidzura

The University of Manchester https://orcid.org/0000-0002-2009-7634

Lindsay Cotterell

The University of Manchester

Poonam Halai

The University of Manchester

Dafydd Thomas

The University of Manchester

Catherine O'Neill

The University of Manchester

Clare O'Connor

No7 Beauty Company, The Boots Group

Mike Bell

No7 Beauty Company, The Boots Group

Article

Keywords:

Posted Date: March 25th, 2026

DOI: https://doi.org/10.21203/rs.3.rs-9150312/v1

License: This work is licensed under a Creative Commons Attribution 4.0 International License.
Read Full License

Additional Declarations: There is **NO** Competing Interest.

Abstract

Human skin comprises diverse epithelial, mesenchymal, immune and appendage-associated cell populations organised within structured spatial niches. Whilst single-cell RNA sequencing defines transcriptional states, it lacks spatial resolution and accurate mapping within intact tissue. Here, we introduce a high-resolution spatial single-cell profiling framework for human skin to achieve comprehensive cellular annotation in situ. This approach resolves transcriptionally similar and low-abundance populations across epidermal, dermal and appendage compartments, including basal and suprabasal keratinocytes, fibroblast subsets, melanocytes, endothelial and mural cells, and resident immune populations. In skin exposed to inflammatory ultraviolet irradiation, the platform delineates the immune infiltrate at single-cell resolution and captures Langerhans cell egress from the epidermis, demonstrating its capacity to resolve dynamic tissue responses. By improving sensitivity, spatial fidelity and cross-compartment coverage, this framework provides a scalable reference atlas of human skin and establishes a foundation for mechanistic interrogation of tissue organisation, niche interactions and inflammatory remodelling.

Main

The skin forms the primary barrier to the external environment and comprises two principal layers: the epidermis and underlying dermis. The epidermis is a stratified epithelium comprising predominantly keratinocytes (90-95% of cells), alongside specialised populations including melanocytes, Merkel cells, Langerhans cells and CD8+ resident memory T cells [1, 2]. Beneath this, the extracellular matrix-rich dermis contains fibroblasts, diverse immune subsets, vascular and lymphatic networks, and skin appendages such as hair follicles, sweat and sebaceous glands. Together, these layers constitute a structurally and cellularly heterogeneous tissue whose composition varies across anatomical sites. The spatial and temporal organisation enables coordinated responses to environmental challenge, injury and stress, orchestrating processes such as wound repair, immune surveillance, and tissue remodelling. Precise identification and phenotyping of these diverse cell populations is therefore essential for understanding skin homeostasis, disease pathogenesis, and the impact of factors such as ageing and ethnicity.

To date, the cellular composition of healthy human skin has largely been defined using single-cell RNAseq (scRNAseq), enabling large-scale transcriptional profiling at single-cell resolution [3-6]. However, these approaches lack spatial context, precluding comprehensive reconstruction of tissue architecture, cellular interactions and niche organisation. In addition, anatomically distinct skin compartments with overlapping transcriptomic signatures cannot be reliably discriminated. Rare or spatially restricted populations may also be underrepresented, and the enzymatic and mechanical dissociation required to generate single cell suspensions can perturb native transcriptomic states [7].

The emergence of spatial transcriptomic technologies has enabled gene expression analysis while preserving tissue architecture [8, 9]. However, array-based platforms such as Visium/VisiumHD (10X Genomics) rely on a grid-based capture strategy that aggregate transcripts from multiple cells, limiting

true single-cell resolution and precise mapping of cellular interactions. Imaging-based approaches, including MERFISH, achieve single-cell resolution and have generated spatial atlases of human skin [10] but depend on targeted gene panels and computational inference of cellular boundaries, which can be challenging in densely packed, structurally complex tissues such as human skin. These limitations highlight the need for approaches that combine robust single-cell resolution with scalable, whole-tissue coverage. The recently developed Xenium platform (10X Genomics) enables imaging-based spatial transcriptomics at single-cell resolution across intact tissue sections using defined gene panels. To date, Xenium has primarily been used to spatially validate or contextualise cell types identified through scRNAseq or Visium [8, 11,]. Here, we extend this application by generating a comprehensive spatial single-cell atlas of human skin using a bespoke panel and integrated protein-guided cell segmentation. This framework enables comprehensive tissue-wide mapping of epidermal, dermal, appendage and immune cell populations across intact human skin sections, establishing a high-resolution, scalable reference applicable to both homeostatic and perturbed states, demonstrated in this study through spatial profiling of ultraviolet-induced inflammatory responses.

Results

Spatial transcriptomic analysis identifies predominant skin cell types

To spatially resolve cellular diversity in human skin, we profiled healthy extensor forearm skin (n=5; Fig 1a) using a 479-gene panel derived from the Xenium Human Skin Gene Expression Panel (10x Genomics) and curated with additional markers from published scRNA-seq datasets to optimise delineation of major skin cell populations.

Following quality filtering (<10 transcripts per cell removed) and merging of the data, 29,060 cells were identified for analysis (Fig. 1a). Integrated UMAP embedding and unsupervised clustering identified 31 clusters corresponding to 10 major cell types (Fig. 1b). Keratinocytes comprised the largest proportion (36.9%) and were resolved into basal (8.3%), suprabasal (16.8%), and non-epidermal (11.8%) subsets. Fibroblasts represented 28.6% of cells, followed by endothelial (10.4%), mural (7.8%), eccrine secretory duct (6.7%), sebocytes (2.1%), melanocytes (1.9%) and immune populations (5.5%) spanning both myeloid and lymphoid lineages (Fig. 1c).

Cell-type annotation was performed using established marker genes (Table 1). To enhance immune cell detection in the absence of canonical pan-leukocyte markers (e.g., PTPRC), curated immune lineage- and cell type-specific gene sets were combined to define a broad immune compartment, which was subsequently resolved into discrete immune subsets. Marker enrichment corresponded with annotated clusters (Fig. 1d), and spatial mapping across whole sections recapitulated tissue architecture, including appendages and vascular structures (Fig. 1e).

Table 1: Genes used to identify each cell type

Cell Type	Genes
Keratinocytes	
Epidermal basal	*DST, COL17A1, POSTN*
Epidermal suprabasal	*DSG1, DSC1, GATA3, KRT2*
Non-epidermal	*FABP5, SOSTDC1, TNC, PTN, GJB2*
Melanocytes	*MLANA, PMEL, TYR, TRPM1*
Fibroblasts:	
Fb1	*COL1A1, COL6A1, FBN1, FN1, COL18A1, COL23A1, APCDD1, PTGDS*
Fb2	*COL1A1, COL6A1, FBN1, FN1, COL12A1, MFAP5, MMP2, THBS2*
Sebocytes	*FADS2, INSIG1, DHCR7*
Eccrine secretory duct cells	*DCD, KRT8, KRT19*
Mural cells	*MYH11, MYL9, ACTA2*
Endothelial cells	*AQP1, CD93, SPARCL1, VWF*
Immune cells:	
Myeloid associated	*LYZ, TYROBP, ITGAX, AIF1, CD68,*
Lymphocyte associated	*LTB, LCK, PTPRCAP, TNFRSF1B, TGFB1, COTL1, CTLA4*
Langerhans cells	*CD1A, CD207, FCER1A*
cDC1	*ITGAX, CPVL, CLEC9A, WDFY4, XCR1*
cDC2	*ITGAX, CPVL, CLEC10A, CD1C*
Macrophages	*CD163, CD14, C1QA, C1QB, C5AR1*
Neutrophils	*MPO, ELANE*
T cells	*CD2, CD52, CD3E, CD3D*
NK cells	*GZMB, GZMK, GNLY, NKG7*
Mast cells	*TPSAB1, CPA3, IL1RL1, GATA2*
B cells	*CD79A, MZB1, TNFRSF17, CD19*

Identification of keratinocyte subtypes and melanocytes

The epidermis comprises a heterogeneous compartment dominated by keratinocytes, alongside melanocytes, and immune populations such as Langerhans cells [12]. Keratinocytes pose a particular challenge for spatial resolution as they are present in both the epidermis and the hair follicles.

Epidermal keratinocytes (basal and suprabasal; 7296 cells) accounted for 8 of the 31 clusters, while non-epidermal keratinocytes (3437 cells) formed 5 distinct clusters (Fig. 2a). Basal keratinocytes were defined by *POSTN*, *COL17A1*, and *DST* expression and localised exclusively to the basal layer (Fig. 2b), whereas suprabasal keratinocytes expressed *DSC1, DSG1, KRT2*, and *GATA3*, and were restricted to suprabasal layers (Fig. 2c). Spatial mapping confirmed coherent organisation of these populations across the epidermis (Fig. 2d) and immunofluorescence staining for COL17A1 and DSC1/DSG1 validated marker specificity (Fig. 2e). Non-epidermal keratinocytes, characterised by *FABP5*, *SOSTDC1*, *PTN*, *TNC*, and *GJB2*, segregated into distinct clusters in the UMAP (Fig. 2f), and localised to hair follicles and eccrine glands, but not the interfollicular epidermis (Fig. 2f, 2g).

Melanocytes (595 cells), defined by *MLANA*, *PMEL*, *TYR*, and *TRPM1*, formed 2 discrete clusters and were spatially confined to the basal epidermis, consistent with established architecture [13] (Fig. 2h, i).

Dot plot analysis demonstrated clear transcriptional separation of basal, suprabasal, and non-epidermal keratinocytes underscoring the capacity of the panel to resolve closely related epidermal subtypes within intact tissue (Fig. 2j).

Identification of cells associated with skin appendages and the vasculature

Skin appendages and the vascular network represent structurally and functionally specialised compartments essential for tissue homeostasis [14].

Sebocytes (n = 598) formed two distinct clusters and localised adjacent to hair follicles (Fig. 3a). These cells exhibited enriched expression of lipid metabolism–associated genes, including *FADS2*, *INSIG1*, and *DHCR7*, with spatially restricted transcript localisation corresponding to sebaceous gland structures *in situ* (Fig. 3b).

Eccrine secretory duct cells (n = 1959) also segregated into two clusters and mapped closely to eccrine gland architecture (Fig. 3c). This population was defined by expression of *DCD*, *CES1*, *KRT8*, and *KRT19*, with spatial enrichment confirmed *in situ* (Fig. 3d).

Within the vascular compartment, 2,267 mural cells were identified by MYH11, MYL9 and ACTA2 expression *(Fig 3e, 3f),* alongside 3,023 endothelial cells defined by *AQP1*, *CD93*, *SPARCL1*, and *VWF (Fig. 3g, h)*. Dot plot analysis demonstrated clear segregation of appendage and vascular marker gene expression across clusters (Fig 3i).

Identification of fibroblast cells and two distinct subtypes

Fibroblasts represented a major stromal population (n = 8321), comprising 5 of 31 clusters (Fig. 4a). Cells were identified using a panel of four well-characterised fibroblast marker genes: *COL1A1, FBN1,*

FN1, and *COL6A1,* consistent with previous reports [9, 15, 16]. Transcript visualisation demonstrated high transcript abundance and co-localisation within individual cells (Fig. 4b) and spatial mapping confirmed restriction to the dermal compartment (Fig. 4c).

Subclustering resolved the fibroblast population into two spatially and transcriptionally distinct subtypes (Fig. 4e). One subtype was predominantly localised to the upper dermis and perifollicular regions and showed enriched expression of *COL18A1, COL23A1, APCDD1,* and *PTGDS*, genes previously associated with papillary dermal fibroblasts [15, 17]. The second subtype was largely found within the deeper dermis and was also observed in proximity to hair follicles and eccrine glands. It exhibited higher expression of *COL12A1, MFAP5, MMP2,* and *THBS2*, genes commonly associated with reticular or matrix-remodelling dermal fibroblast populations [15, 16], alongside comparatively low expression of papillary-associated genes (Fig. 4d).

Identification of immune cells and subtypes

Broad cell-type annotation identified 1,594 immune cells across five skin samples, resolving nine principal subsets: Langerhans cells, macrophages, mast cells and two dermal dendritic cell populations comprised much of the immune compartment, with B cells, T cells, natural killer (NK) cells, and neutrophils also identified at lower numbers (Fig. 5b). Langerhans cells (309 cells) localised predominantly to the epidermis, with occasional follicular localisation, and were defined by *CD1A*, *FCER1A*, and *CD207* expression, with *CD207* providing the most robust marker signal [1] (Fig. 5c-d). Macrophages (701 cells) were distributed throughout the dermis and in association with adnexal structures, and expressed *CD163, CD14, C1QA, C1QB and CD5AR1*. Mast cells (390 cells) localised to the dermis, including the perifollicular niche and surrounding eccrine glands, were characterised by *TPSAB1, CPA3, IL1RL1* and *GATA2* expression. Conventional dendritic cells (cDCs) (144 cells), located throughout the dermis, were characterised by expression of *ITGAX* (encoding CD11c) and *CPVL*, forming two principal populations consistent with type 1 (cDC1) and type 2 (cDC2) dendritic cells, based on established markers. cDC1 expressed *CLEC9A, WDFY4,* and *XCR1*, whereas cDC2 exhibited higher *CLEC10A* and *CD1C* expression (Fig. 5c-d). Neutrophils were identified by expression of *MPO* and *ELANE* and found at very low abundance (2 cells across 5 sections), consistent with healthy baseline skin. T cells (43 cells) and NK cells (4 cells) were also detected at low frequency. T cells expressed *CD2, CD52, CD3E* and *CD3D* and were detected in both the epidermis and dermis, while NK cells were defined by *GNLY, CTSW, NCAM1* and *NKG7* (Fig. 5c-d). A single B cell was identified based on *CD79A, MZB1, TNFRSF17* and *CD19* expression (Fig. 5c) Given their low abundance in healthy skin, neutrophils, B cells, T cells and NK cells were resolved only after immune-specific subclustering with per-cell annotation rather than cluster-level assignment.

Spatial profiling of ultraviolet radiation-induced inflammation in human skin

To confirm our approach could sensitively detect and spatially resolve immune populations under inflammatory conditions, we analysed human skin following an acute inflammatory stimulus. Upper back skin was exposed to an inflammatory (sunburn) dose of solar-simulated ultraviolet radiation (UVR), then samples of irradiated and non-irradiated skin from the same donor were processed using the same analytical pipeline described above.

We identified 8,877 cells in non-irradiated skin and 12,279 in irradiated skin, with irradiated skin exhibiting a higher proportion of immune cells (15.86%; 2,018 cells) compared with non-irradiated skin (4.51%; 400 cells), consistent with an inflammatory infiltrate [18]. Other increases in total cell number were likely attributed to anatomical heterogeneity between cryosections, including deeper dermal sampling and the presence of a prominent hair follicle (Fig. 6a-c).

Spatial mapping revealed pronounced immune cell accumulation within the upper dermis, including a prominent immune cell cluster located directly beneath the epidermis. Despite close spatial proximity, distinct myeloid and lymphoid subsets were clearly resolved (Fig. 6c). In line with established UVR-induced migration dynamics [19], Langerhans cells were readily detected within the epidermis of non-irradiated skin but were absent following irradiation (Fig. 6d).

Discussion

Here, we present a targeted, single-cell resolution spatial atlas of human skin generated using an integrated, end-to-end analytical framework. By combining curated gene panel design, high resolution spatial transcriptomics and robust protein-guided segmentation, this approach enables scRNA-seq–style clustering and subsetting of data while preserving native tissue architecture, eliminating the need for cross-platform data integration.

This unified strategy improves annotation accuracy in cell dense, highly structured tissue, enhances detection of low abundance populations and permits confident spatial assignment of transcriptionally similar cell types. Importantly, we demonstrate performance beyond homeostatic tissue. Application to UVR-induced inflammation revealed dynamic immune remodelling, including dermal immune accumulation and Langerhans cell egress from the epidermis[19]. These findings establish the framework as applicable not only to healthy tissue mapping but also to perturbed states, including inflammatory, disease and treatment contexts where accurate resolution of rare or infiltrating populations is essential.

Panel design was informed by prior single-cell studies of human skin [9, 15, 20] but refined through iterative spatial validation. Several canonical markers (including *KRT1*, *KRT10*, *VIM* and *HLA-DRA*) were excluded due to panel design constraints or insufficient spatial specificity. Notably, commonly used basal keratinocyte markers *KRT5 and KRT15* [21] were not selected for our panel as spatial assessment of transcript distributions revealed *KRT5* and *KRT15* expression was not confined to the epidermis but could be detected in non-epidermal keratinocyte-containing appendages, including hair follicles and eccrine glands (Supplementary Fig. 2), underscoring the importance of spatially informed marker

selection. Iterative optimisation enabled robust cell-type delineation without reliance on these genes, highlighting the necessity of integrating spatial context into panel curation.

Several spatial transcriptomic technologies have been applied to human skin. Restrepo et al. used a MERFISH-based framework to resolve spatial organisation and infer cellular communication [10]. While this approach achieved high-resolution mapping, reliable identification of rare populations, including NK cells, remained challenging. Similarly, Stereo-seq offers whole-transcriptome coverage with high theoretical resolution [22]; however, practical implementation often requires aggregation of spatial signals into defined bins, and the lack of integrated cell segmentation can limit accurate transcript-to-cell assignment in densely populated tissues. In contrast, our Xenium-based framework combines targeted, high-sensitivity profiling with protein-guided segmentation, enabling confident transcript assignment at subcellular resolution. This strategy supports reliable detection of low-abundance populations, including NK cells, and robust discrimination of closely apposed cell types within complex skin microenvironments.

When applying or adapting this framework to other contexts, several factors merit consideration. First, this study examined extensor forearm skin as a structurally intact representative anatomical site that encompasses the full complement of major skin cell types and appendages. Regional variation in architecture and transcriptional programmes across body sites would be expected and should be considered when extrapolating these findings (e.g., compared with more protected sites such as the buttock [23]). Second, as a targeted spatial platform, gene selection is necessarily constrained by the 480-gene capacity of the system. While this does not provide whole-transcriptome coverage, it enables highly curated, hypothesis-driven panel design with enhanced sensitivity and spatial fidelity. Although a larger set of transcripts contributed to transcriptional variation and cluster separation, only 85 canonical markers were required for cell-type annotation, leaving substantial capacity within the panel for additional genes tailored to specific biological or disease-focused applications.

In summary, we establish a scalable, spatially resolved single-cell reference of human skin and provide a generalisable framework for high-fidelity tissue mapping, while also enabling detection of rare resident and infiltrating cell populations, subsets of major cell types and precise resolution of closely clustered cell types. This platform enables mechanistic interrogation of tissue organisation, niche interactions and inflammatory remodelling, and offers a flexible foundation that can be readily adapted by modification of the panel to suit specific biological questions or disease-focused applications.

Methods

Participants and tissue samples

Samples of healthy human skin from the extensor forearm were obtained by punch biopsy (3mm diameter) from n=5 healthy adults aged 34-40 years (4 females, 1 male). A sixth participant (age 24, male) provided punch biopsy samples from UVR exposed and unexposed areas of the upper back. All

participants had a “light” Individual Typology Angle skin type. The study was approved by The University of Manchester Research Ethics Committee (references: 2025-19295 and 2022-12972). Participants provided written informed consent, and the study was performed according to the principles of the Declaration of Helsinki.

Irradiation of human skin

Upper back skin was exposed to 80 mJ/cm² erythemally weighted solar simulated UVR using an Oriel SOL-UV-6 Solar Simulator (Newport corporation; emission range 290-400nm). At 24 hours post-irradiation, punch biopsies (5mm diameter) were collected from irradiated skin and from a non-irradiated site on the contralateral side.

Spatial transcriptomic data generation

Spatial gene expression profiling of human tissue samples was performed using the Xenium In Situ platform (10x Genomics) following the manufacturer’s protocols and using a custom designed 479 skin-specific gene panel curated from the 10X Genomics predesigned skin panel and published scRNA-seq datasets.

Spatial transcriptomic data analysis

All analyses were performed in R (version ≥4.3). Xenium output files were analysed using the Seurat package using standard spatial transcriptomic workflows. Subsequent quality control retained cells containing between 10 and 479 detected genes and between 10 and 3,000 total transcript counts. Data were normalised using SCTransform (v2). Principal component analysis generated 15 principal components that were used to construct a shared nearest-neighbour graph based on an elbow plot (Supplementary figure 1), followed by dimensionality reduction using uniform manifold approximation and projection (UMAP). Unsupervised clustering was performed at a resolution of 1.0.

Cell type annotation

Following per-cell module scoring, automated cell type assignment was carried out. Each cell was assigned to the cell type corresponding to its highest module score based on the cell typing gene list (Table 1).

Immunofluorescence

Immunofluorescence staining was performed on consecutive skin tissue sections to validate spatial transcriptomic identification of epidermal keratinocyte subsets and melanocytes. For melanocytes,

tissue sections were fixed with ice-cold acetone, and for keratinocytes, sections were fixed with neutral buffered formalin (10%). Sections were permeabilised with 0.5% Triton X-100, blocked with normal horse serum and incubated with anti-MLANA (ab51061; Abcam), anti-COL17A1(ab184996; Abcam), anti-DSG1 (690092, Progen), DSC1(ab209490; Abcam) for 1 hour at room temperature. Following washing, species-appropriate fluorophore-conjugated secondary antibodies (Vector Labs) were applied and then sections were mounted in fluoromount with DAPI. Images were acquired using fluorescence microscopy (Evident, CellSens).

Declarations

Acknowledgements

This work was supported by a Biotechnology and Biological Sciences Research Council Prosperity Partnership Award [BB/Y003233/1] to No7 Beauty Company/The Boots Group and The University of Manchester. C.O'N., A.K.L. and M.F. are supported by the National Institute for Health and Care Research (NIHR) Manchester Biomedical Research Centre (BRC) (NIHR203308).

Author contributions

M.P., B.M. and A.K.L. conceived the study. A.L and M.F directed the study. L.C., A.C., P.H. and W.D. acquired volunteer samples. M.P., B.M. and D.T. generated spatial transcriptomics datasets. M.P. and B.M. performed the bioinformatics analysis. O.K. performed immunofluorescence staining. M.P., B.M., C.O'C., M.B., C.O'N., M.F. and A.K.L. contributed to data interpretation. All authors read and approved the content of this manuscript.

Data availability

Xenium data and full gene panel used in this study are available from https://figshare.com/s/bf1c0a6330ec0e876d46

Code availability

The code generated during this study is available at GitHub at https://github.com/langtonlab/skin-cell-atlas.git

References

1. Doebel, T., Voisin, B. & Nagao, K. Langerhans cells – the macrophage in dendritic cell clothing. *Trends Immunol* **38**, 817-828 (2017).

2. Wright, M.C. et al. Merkel cells are long-lived cells whose production is stimulated by skin injury. *Dev Biol* **422**, 4-13 (2017).
3. Reynolds, G. et al. Developmental cell programs are co-opted in inflammatory skin disease. *Science* **371**, eaba6500 (2021).
4. Ahlers, J.M.D. et al. Single-cell RNA profiling of human skin reveals age-related loss of dermal sheath cells and their contribution to a juvenile phenotype. *Frontiers in Genet* **12** (2022).
5. Zou, Z. et al. A single-cell transcriptomic atlas of human skin aging. *Dev Cell* **56**, 383-397.e388 (2021).
6. He, H. et al. Single-cell transcriptome analysis of human skin identifies novel fibroblast subpopulation and enrichment of immune subsets in atopic dermatitis. *J Allergy Clin Immunol* **145**, 1615-1628 (2020).
7. Burja, B. et al. An optimized tissue dissociation protocol for single-cell RNA sequencing analysis of fresh and cultured human skin biopsies. *Front Cell Dev Biol* **10** (2022).
8. Steele, L. et al. A single-cell and spatial genomics atlas of human skin fibroblasts reveals shared disease-related fibroblast subtypes across tissues. *Nat Immunol* **26**, 1807-1820 (2025).
9. Ganier, C. et al. Multiscale spatial mapping of cell populations across anatomical sites in healthy human skin and basal cell carcinoma. *Proc Natl Acad Sci U S A* **121**, e2313326120 (2024).
10. Restrepo, P. et al. A single-cell spatial transcriptomic census of human skin anatomy. *bioRxiv*, 2025.2009.2022.676865, https://doi.org/676810.671101/672025.676809.676822.676865 (2025).
11. Janesick, A. et al. High resolution mapping of the tumor microenvironment using integrated single-cell, spatial and in situ analysis. *Nat Commun* **14**, 8353 (2023).
12. Baroni, A. et al. Structure and function of the epidermis related to barrier properties. *Clin Dermatol* **30**, 257-262 (2012).
13. Cichorek, M., Wachulska, M., Stasiewicz, A. & Tymińska, A. Skin melanocytes: biology and development. *Postepy Dermatol Alergol* **30**, 30-41 (2013).
14. Hosseini, M., Koehler, K.R. & Shafiee, A. Biofabrication of human skin with its appendages. *Adv Healthc Mater* **11**, e2201626 (2022).
15. Solé-Boldo, L. et al. Single-cell transcriptomes of the human skin reveal age-related loss of fibroblast priming. *Commun Biol* **3**, 188 (2020).
16. Deng, C.-C. et al. Single-cell RNA-seq reveals fibroblast heterogeneity and increased mesenchymal fibroblasts in human fibrotic skin diseases. *Nat Commun* **12**, 3709 (2021).
17. Philippeos, C. et al. Spatial and single-cell transcriptional profiling identifies functionally distinct human dermal fibroblast subpopulations. *J Invest Dermatol* **138**, 811-825 (2018).
18. Strickland, I., Rhodes, L.E., Flanagan, B.F. & Friedmann, P.S. TNF-alpha and IL-8 are upregulated in the epidermis of normal human skin after UVB exposure: correlation with neutrophil accumulation and E-selectin expression. *J Invest Dermatol* **108**, 763-768 (1997).

19. Achachi, A. et al. UV radiation induces the epidermal recruitment of dendritic cells that compensate for the depletion of langerhans cells in human skin. *J Invest Dermatol* **135**, 2058-2067 (2015).
20. Wang, S. et al. Single cell transcriptomics of human epidermis identifies basal stem cell transition states. *Nat Commun* **11**, 4239 (2020).
21. Redmond, C.J. et al. Keratin 15 promotes a progenitor cell state in basal keratinocytes of skin epidermis. *J Cell Biol* **225** (2026).
22. Li, Y. et al. High-resolution spatial transcriptomics unveils spatially resolved gene modules and fatty acid metabolism dysregulation in human skin aging. *J Invest Dermatol* **146**, 640-653.e648 (2026).
23. Langton, A.K., Graham, H.K., Griffiths, C.E.M. & Watson, R.E.B. Ageing significantly impacts the biomechanical function and structural composition of skin. *Exp Dermatol* **28**, 981-984 (2019).

Figures

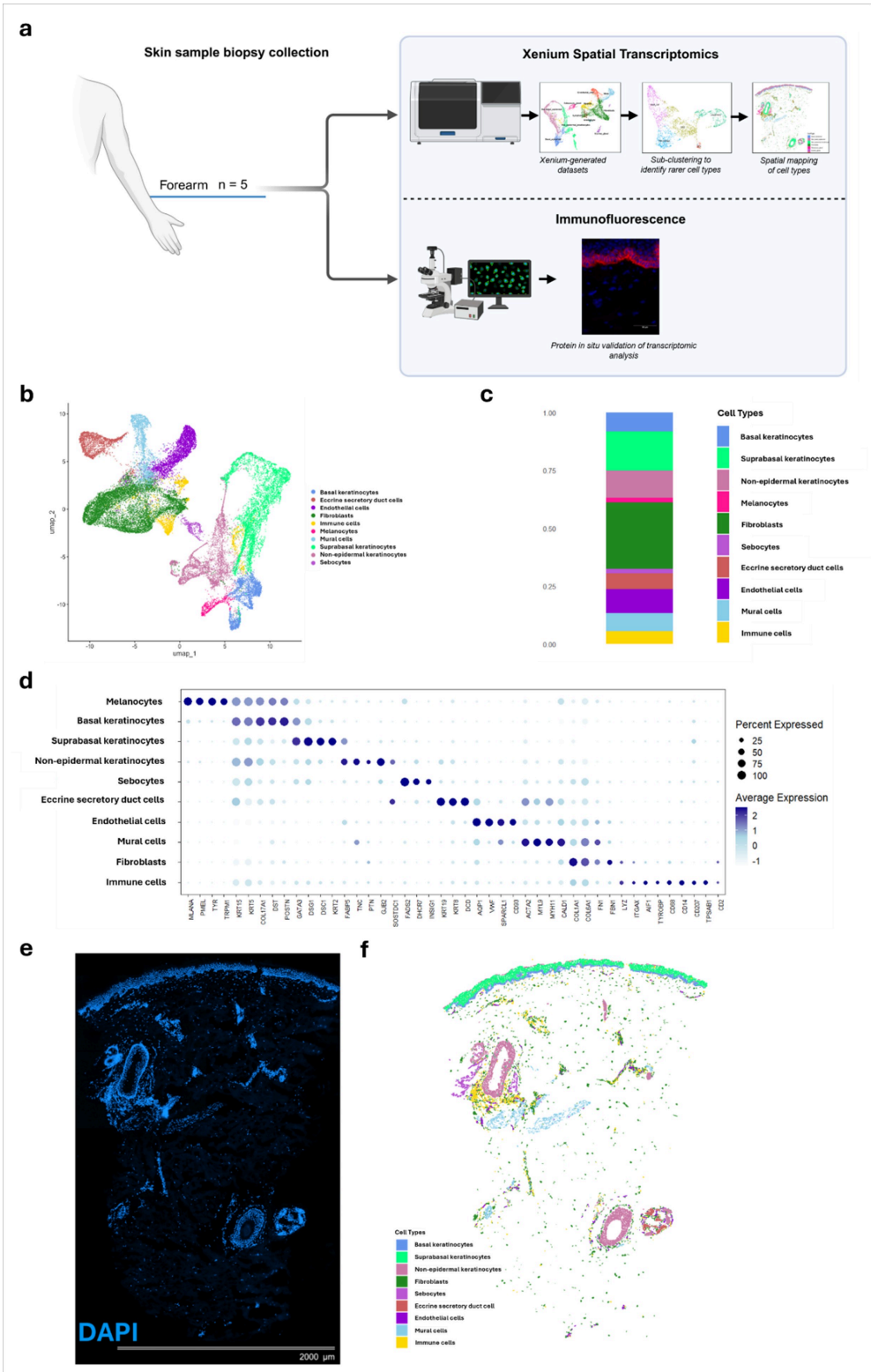


Figure 1

Study overview and identification of broad cell types in human skin

a,*Study methodology, including sites of sample collection from human forearm and downstream analysis (Created with Biorender)* ***b,*** *Uniform Manifold Approximation and Projection (UMAP) showing major skin cell types.* ***c****, Proportions of major skin cell types.* ***d,*** *Expression dot plot of all genes used for*

major cell type identification. ***e,*** *Representative 4',6-diamidino-2-phenylindole (DAPI) staining of a skin section imaged using Xenium Explorer (v4.1.1).* ***f,*** *Representative example of spatial mapping of the 10 identified major cell types in a single section of skin*

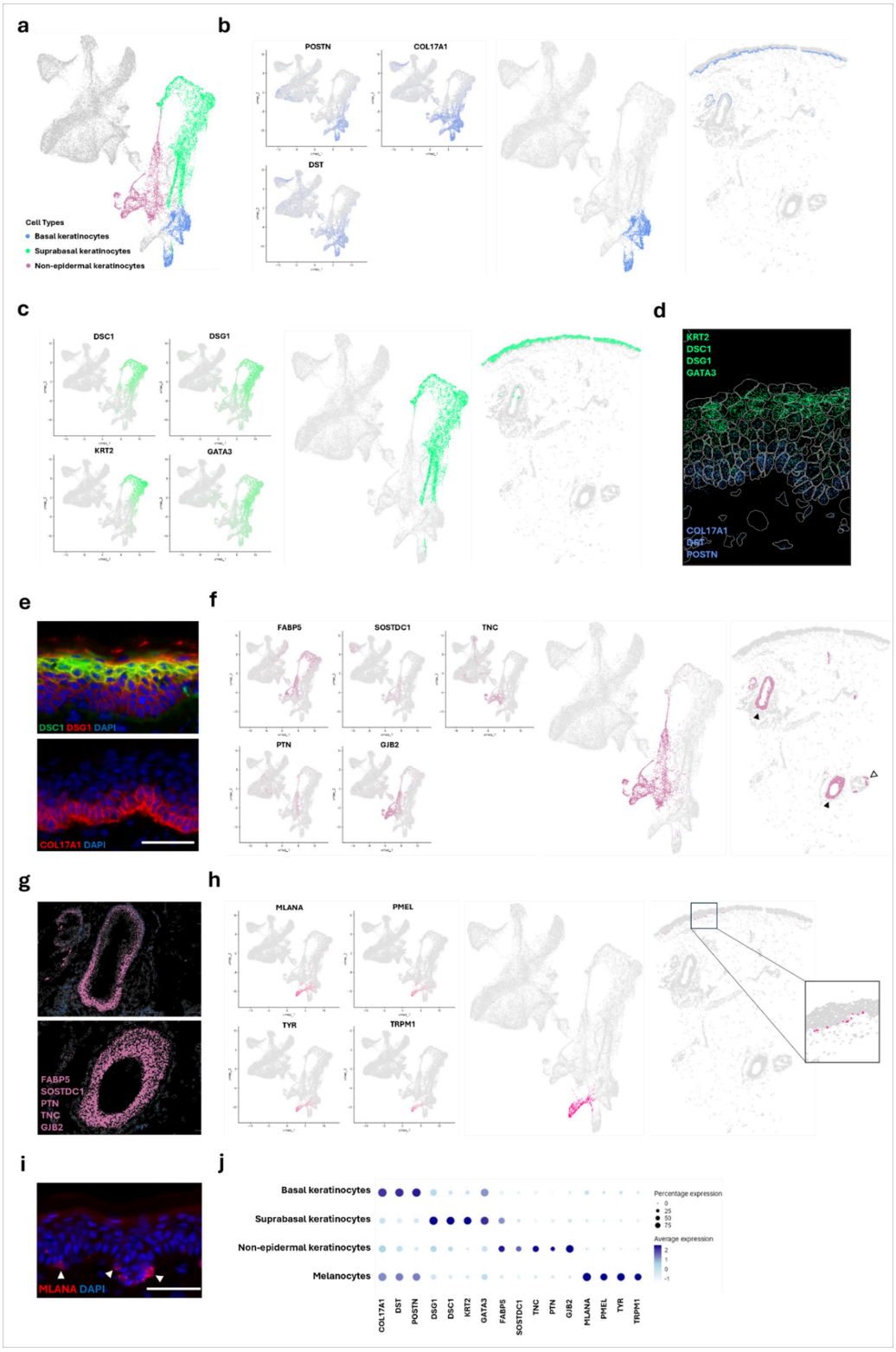


Figure 2

Identification of keratinocyte populations and melanocytes in human skin.

a,*UMAP clustering of integrated datasets showing epidermal and non-epidermal keratinocytes.* ***b,*** *UMAP clustering and spatial localisation of basal keratinocytes expressing POSTN, COL17A1, and DST.* ***c,*** *UMAP and spatial localisation of suprabasal keratinocytes expressing DSC1, DSG1, KRT2, and GATA3.* ***d,*** *In situ mapping of selected epidermal transcripts showing coherent spatial organisation.* ***e,*** *Immunofluorescence validation of COL17A1 and DSC1/DSG1 expression.* ***f,*** *UMAP clustering of non-epidermal keratinocyte clusters with spatial mapping indicating non-epidermal keratinocytes in mainly hair follicles (black arrowhead) and some expression in the eccrine gland (white arrowhead).* ***g,*** *In situ localisation of non-epidermal keratinocyte markers (FABP5, SOSTDC1, TNC, PTN, GJB2) to hair follicles.* ***h,*** *UMAP clustering and spatial localisation of melanocytes expressing MLANA, PMEL, TYR, and TRPM1.* ***i,*** *Immunofluorescence validation of melanocytes using MLANA (white arrows). Scale bar = 50 µm.* ***j,*** *Dot plot showing marker gene expression across basal, suprabasal, non-epidermal keratinocytes and melanocytes. Percentage expression represents the proportion of cells that express the gene within the identified cell population and average expression is the mean intensity of the gene transcript level across expressing cells. In situ maps were generated with Xenium Explorer (v4.1.1).*

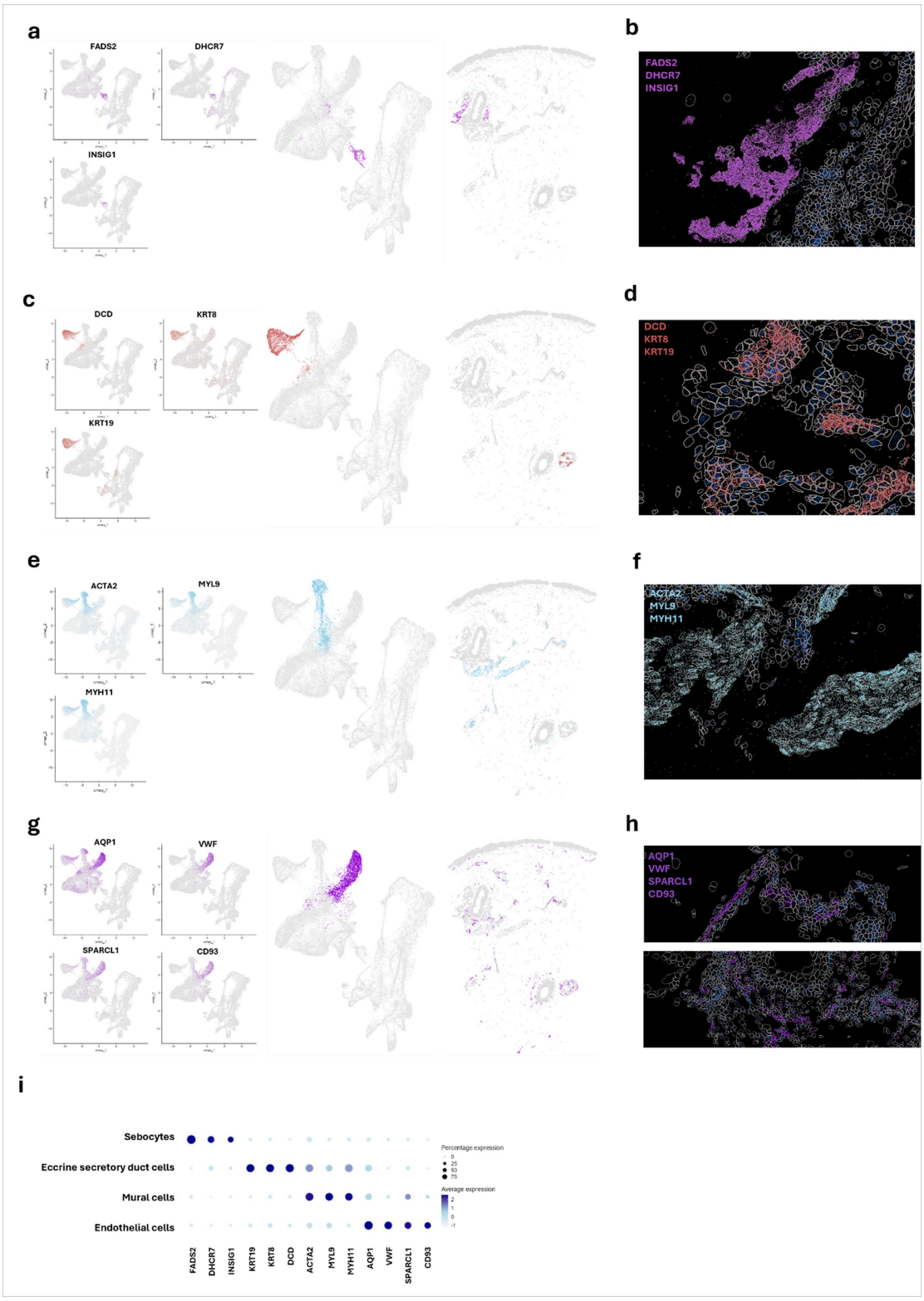


Figure 3

Identification of skin appendage cell populations in human skin.

a,*UMAP clustering and spatial localisation of sebocytes.* ***b,*** *In situ expression of lipid metabolism–associated genes (FADS2, DHCR7, INSIG1) in sebocytes.* ***c,*** *UMAP clustering and spatial projection of eccrine gland cells.* ***d,*** *In situ localisation of eccrine secretory duct cells markers (DCD, CES1, KRT8,*

*KRT19). **e,** UMAP clustering and spatial localisation of mural cells expressing MYH11, MYL9, and ACTA2. **f,** In situ mapping of mural cell identifying transcripts. **g,** UMAP clustering of endothelial cells expressing AQP1, CD93, SPARCL1, SPARCL1, and VWF. **h,** In situ transcript localisation in endothelial cells. **i,** Dot plot showing marker gene expression across skin appendage cell populations. Percentage expression represents the proportion of cells that express the gene within the identified cell population and average expression is the mean intensity of the gene transcript level across expressing cells.In situ maps were generated with Xenium Explorer (v4.1.1).*

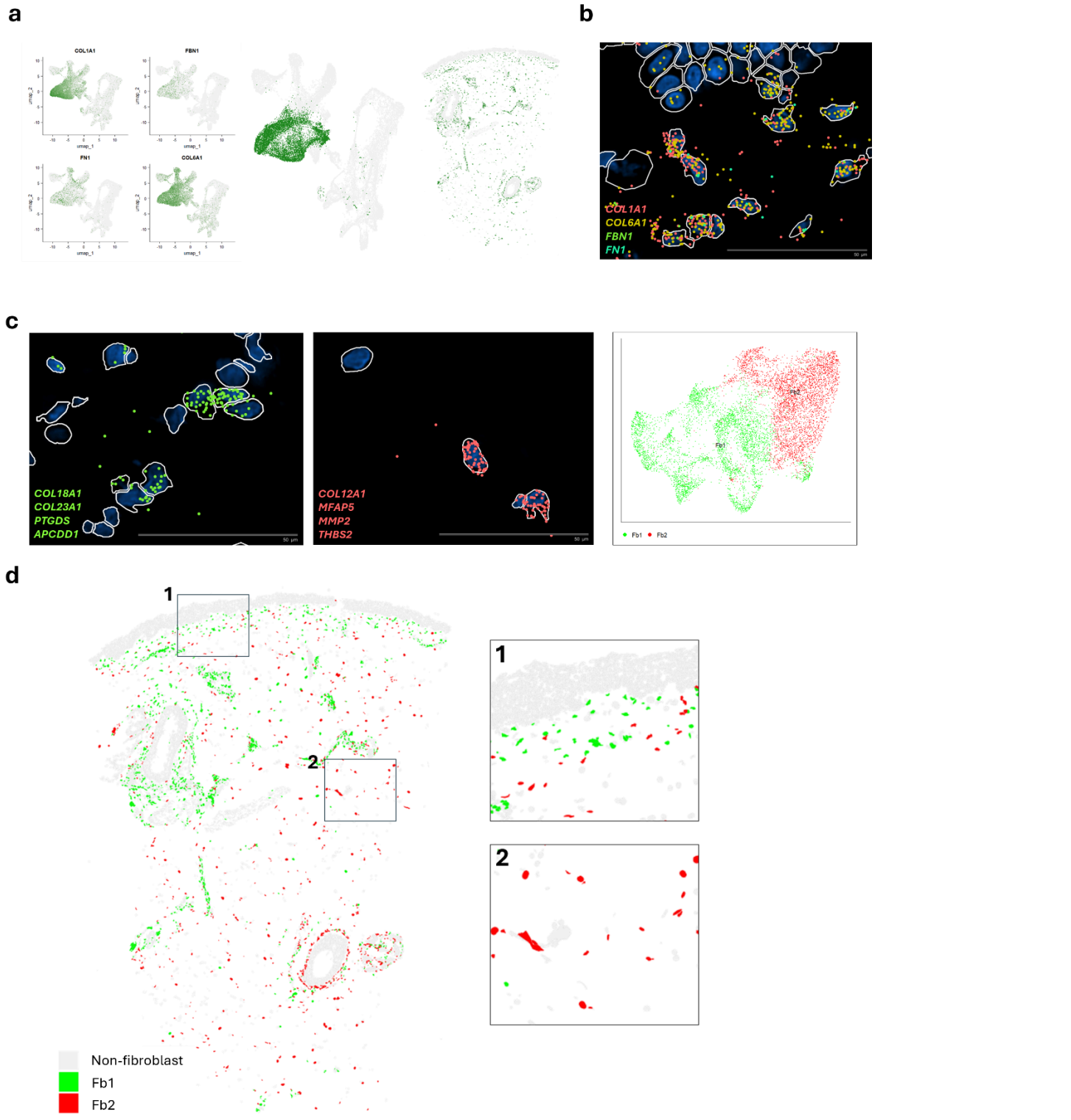


Figure 4

Identification of fibroblast subtypes in human skin

a, *Spatial localisation of fibroblasts expressing COL1A1, FBN1, FN1, and COL6A1.* ***b,*** *Transcript location of fibroblast marker genes from the Xenium Explorer software (v4.1.1).* ***c,*** *Transcriptomic localisation of marker genes defining two distinct fibroblast subpopulations (left), alongside UMAP embedding of fibroblasts resolved into Fb1 and Fb2 subsets.* ***d,*** *Representative images showing the spatial localisation of fibroblast subtypes Fb1 and Fb2.*

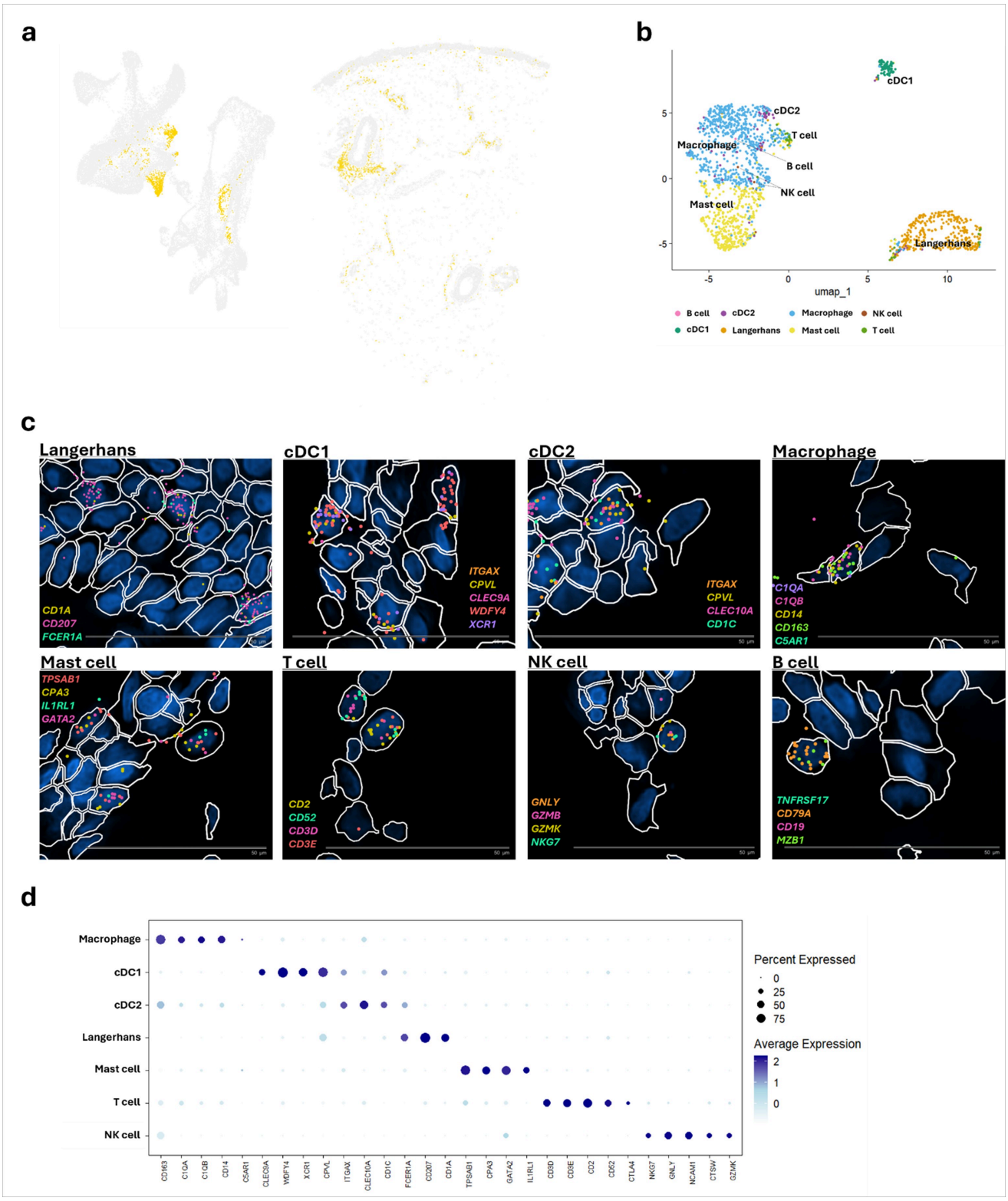


Figure 5

Identification of immune populations in human skin

a,*Spatial localisation of immune cells.* ***b,*** *UMAP of immune subtypes within 5 healthy individuals.* ***c,*** *Gene marker transcript location for each immune cell subtype.* ***d,*** *Dot plot of marker gene expression for*

identified immune cell subtypes within forearm skin. In situ maps were generated with Xenium Explorer (v4.1.1).

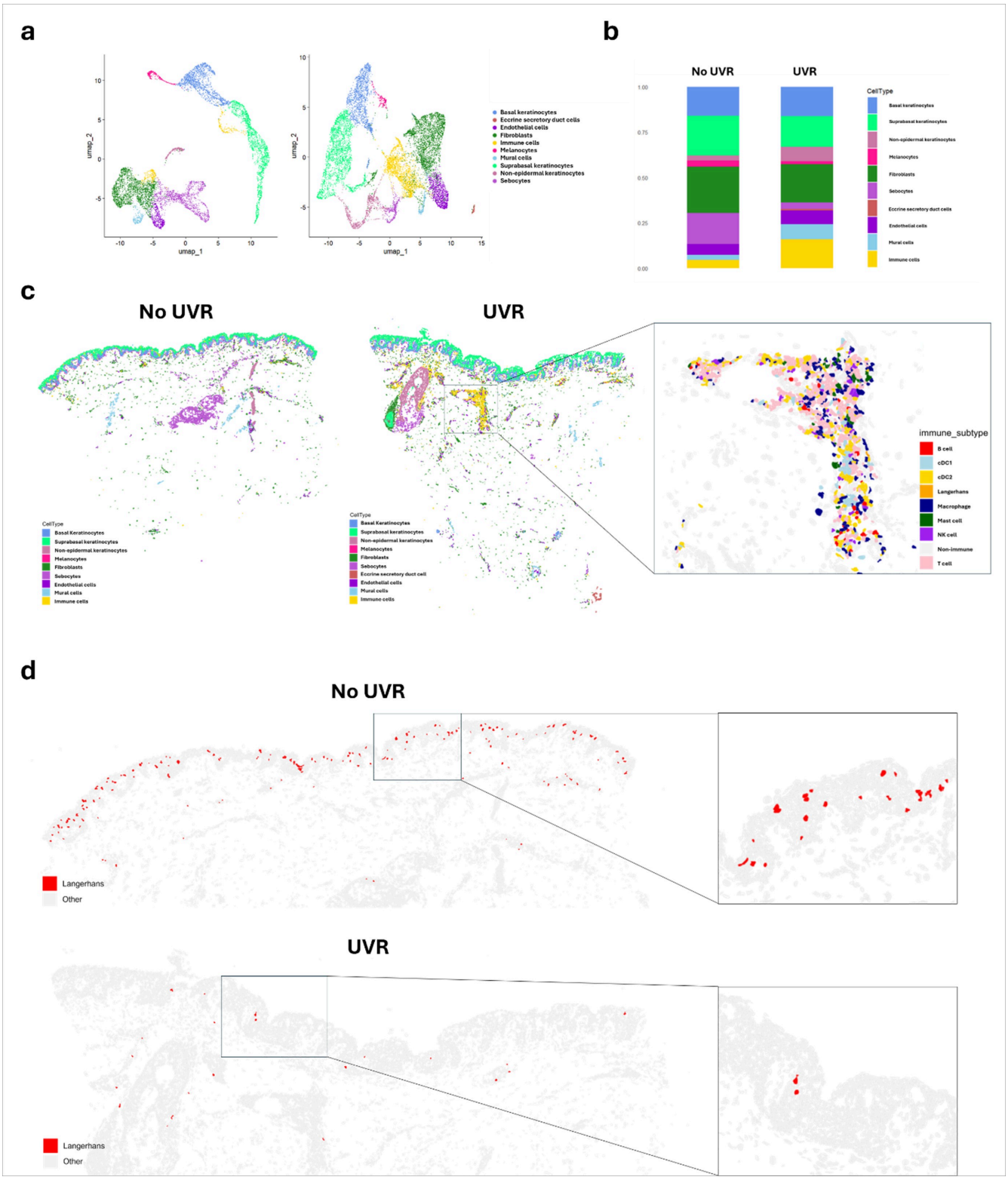


Figure 6

Identification of immune populations in UVR irradiated skin ***a,*** *UMAP embedding of whole cell annotation for skin that is non-irradiated (left) or irradiated with UVR (right).* ***b,*** *Cell proportions in skin with no UVR or UVR.* ***c,*** *Spatial location of broad cell types in non-irradiated (left) or irradiated with UVR (right), with*

defined immune cell types within an immune cell cluster. ***d,*** *Spatial location of Langerhans cells in non-irradiated (top) or irradiated with UVR (bottom).*

Supplementary Files

This is a list of supplementary files associated with this preprint. Click to download.

- SupplementaryFigures.docx